Journal of Structural Geology, Vol. 13, No. 1, pp. 3 to 20, 1991
Printed in Great Britain

0191-8141/91 $03.00+0.00

Centrifuge modelling of fold–thrust structures in a tripartite stratigraphic succession

JOHN M. DIXON

Experimental Tectonics Laboratory, Department of Geological Sciences, Queen's University, Kingston, Ontario, Canada K7L 3N6

and

REIN TIRRUL*

Geological Survey of Canada, Ottawa, Canada

(*Received* 1 *September* 1988; *accepted in revised form* 15 *May* 1990)

Abstract—Analog models measuring 127 × 76 mm in plan were deformed at 2500–4000 **g** in a centrifuge. Scaled stratigraphic sequences were constructed of anisotropic multilayers with individual layers of Plasticine and silicone putty as thin as 40 μm. The plasticine–silicone putty multilayers are analogs for interbedded competent carbonates and clastics, and incompetent pelites, given the model ratios of acceleration, 2500 **g**; length, 5×10^{-6}; specific gravity, 0.6; time 10^{-10}.

Modelling of fold–thrust tectonics emphasizes the influence of stratigraphic succession on structural evolution. The models are constructed with a tripartite stratigraphic succession comprising basal and upper, well-laminated and incompetent units, and a middle, somewhat more isotropic and competent unit. The models deform by three mechanisms: layer-parallel shortening, folding and thrust faulting. They reproduce a number of fold–thrust relationships that have been observed in nature. Folds are typically periclinal, in en échelon arrays. Folds and thrusts are arcuate in plan, reflecting differential shortening. Fold attitudes grade from upright at high levels to overturned at deeper levels within a structural panel, reflecting drag against the basal décollement; fold axial surfaces and thrust faults are listric. While competent units may be offset by localized displacement on thrust faults, the discrete faults may die out both upwards and downwards into regions of ductile strain in less-competent units. Thrust faults appear to follow staircase trajectories through the strata, transecting incompetent units at shallow angles to bedding and competent units at steeper angles. However, the apparent staircase pattern results from propagation of a fault along a relatively straight trajectory through previously-folded strata. Foreland-verging thrusts are more common than back thrusts; the latter have steeper dips.

The models suggest a mechanism of thrust-ramp nucleation following detachment folding: long-wavelength buckling of a competent unit can initiate localized strain (folding and layer-parallel shear) in an underlying incompetent unit, beneath the anticlines of the competent unit; thrust faults propagate up-section from these high-strain zones through the foreland-dipping limbs of buckle-folds in the competent unit. This mechanism may explain the commonly-observed spatial periodicity of thrust ramps.

The model results bear similarities to natural fold–thrust belts in which the stratigraphic succession consists of three mechanical units, for example, the Asiak Foreland and Bear Creek Hills fold–thrust belts of the Slave Province, Northwest Territories, Canada.

INTRODUCTION

Internal geometry of fold–thrust belts

FOLD–THRUST belts form when horizontally layered successions of sedimentary rock are deformed at or near convergent tectonic plate margins. Fore-arc- and back-arc-basin deposits and miogeoclinal prisms are the typical grist for the convergent mill. The stratified sequence is horizontally shortened and vertically thickened by three complementary mechanisms: the pile undergoes uniform layer-parallel shortening; the strata are buckled into fold structures; and the stratigraphic succession is imbricated by displacement on low-angle overthrust faults.

The internal structure of numerous fold–thrust belts has by now been elucidated in detail (see, for example, Faill 1969, Dahlstrom 1970, Price & Mountjoy 1970, Harris & Milici 1977, Laubscher 1977, Suppe 1980, Dixon 1982, Tirrul 1983, to cite only a few), and a number of generalizations can be made. Fold–thrust belts commonly consist of a series of arcuate salients, convex towards the foreland, perhaps reflecting differential shortening across the belt or differential resistance to slip on the underlying décollement horizon. Thrust faults are listric in profile; they may bifurcate upwards into splays, but commonly merge together into master or sole faults at depth. Foreland-verging thrusts are more common than back thrusts; the latter have steeper dips. Thrust faults typically follow stairstep trajectories through the strata, transecting incompetent units at shallow angles to bedding and competent units at steeper angles. First-order folds are intimately associated with thrust faults, many being spatially related to sites where faults ramp upwards across lithologic layering. Displacement varies along the strike length of individual faults, from a maximum near the middle to a minimum at the ends (Elliott 1976); fault displacement

*Deceased 19 May 1987.

typically decreases both up-dip and along strike into the core of a fold (Heim 1921).

In the same way that fault displacement varies along strike, folds are typically periclinal in form and distributed (in map view) in en échelon arrays. Mesoscopic folds commonly range in attitude from upright at high levels to overturned at deeper levels within a structural panel, reflecting drag against the underlying surface of dècollement. While competent units may be offset by displacement on thrust faults, the faults may die out both upwards and downwards into regions of ductile strain in less-competent units.

Relationships between folds and thrusts

The relationship between folding and thrusting in fold–thrust belts has been interpreted in a number of ways. In the early days most workers viewed thrust faults as having formed from pre-existing buckle folds caused by layer-parallel compression (e.g. Rogers & Rogers 1843, Heim 1878, Willis 1894), the faults often propagating from breaks through fold limbs in competent beds. Detachment folds (Jamison 1987), which form above the tip of a bedding-parallel zone of décollement, fall into this category. Buxtorf (1915), in contrast, concluded that low-angle reverse faulting may produce associated drag folds. Folds can also be formed passively by translation of a thrust plate over a ramp (Rich 1934). This 'ramp anticline' or 'fault-bend fold' mechanism has been analysed geometrically (Boyer & Elliott 1982, Suppe 1983) and mechanically (Berger & Johnson 1980, Wiltschko 1981). Although applicable to many fold–thrust complexes, it does not adapt to all cases (e.g. Wiltschko & Chapple 1977, Colman-Sadd 1978, Fox 1983, Reks & Gray 1983). De Sitter (1956) and Dahlstrom (1969) pointed out the need for a thrust below the centre of curvature of a parallel fold; this geometric requirement has been rigorously explored for the case of kink-band 'fault-propagation folding' by Suppe (1985). Jamison (1987) presented geometric criteria for distinguishing among fault-bend, fault-propagation and detachment folds. Factors that control formation of regularly-spaced imbricate thrusts, in the absence of earlier buckling, have been analysed by Mandl & Shippam (1981). Bombolakis (1986) proposed that frontal ramps can propagate serially with regular spacing by a dynamic, stick–slip mechanism. Eisenstadt & De Paor (1987) proposed that the flat–ramp–flat trajectory of thrust faults arises from upward and downward propagation of ruptures that nucleate as ramps in planar competent beds.

Previous model studies

Analog modelling of folding and thrusting dates back some 200 years (Hall 1815 described modelling done in 1788, Cadell 1889, Willis 1894, Bucher 1956). These early studies failed to achieve a reasonable degree of geometric, rheologic and/or dynamic similitude between models and prototypes. This is reflected in the 'unnatural' appearance of model structures. For example, folds grew to excessive amplitude, fold and thrust–fault complexes tended to 'pile up' in front of the advancing platen, and folds developed open spaces in their cores, all because body forces due to gravity were not scaled with the same model ratio as surface forces.

Dennis & Häll (1978) and Guterman (1980) obtained more realistic results by the technique of centrifuge modelling (Hubbert 1937, Ramberg 1967, 1981), which allows body and surface forces to be scaled with the same ratio. Nevertheless, geometric scaling was poor: layers of the order of 0.25–1.0 mm thick represented prototype mechanical units hundreds of metres thick, and in consequence the bending resistance of individual layers likely influenced deformation of the model multilayer much more than in natural prototypes where shear in incompetent interbeds during flexural-slip folding is an important deformation mechanism.

Recently there has been renewed interest in the mechanics of formation of fold–thrust belts and accretionary wedges. Davis *et al.* (1983) analysed the process assuming that the material in the sedimentary pile exhibits cohesive Coulomb behaviour. They also modelled imbricate thrusting in accretionary wedges by subjecting stratified sand to a "push from the rear". Mulugeta & Koyi (1987) extended this type of model study in a detailed examination of the three-dimensional geometry and kinematics of piggy-back thrusting. Mulugeta (1988a) very elegantly demonstrated the importance of correctly scaling body and surface forces in his description of a piston-cylinder squeeze-box for use in a centrifuge. Mulugeta (1988b) modelled the geometry of Coulomb thrust wedges using both 1-**g** squeeze-box and higher-**g** centrifuged experiments. Sand models exhibit (cohesive) Coulomb behaviour. They develop imbricate faults but their passive layering suppresses the development of buckle folds. They are thus not representative of fold-thrust belts in which the stratigraphic pile consists of strata of alternating competence.

The present contribution

This paper presents experimental models in which many of the above-mentioned structural relationships are reproduced. The models are illuminating in that the evolution of the structures can be followed as the models are progressively deformed. The models described here are constructed with a simple tripartite stratigraphic succession, a competent middle unit under- and overlain by less-competent units. The model construction technique employed also permits the incorporation of stratigraphic complexities such as lateral thickness variations and facies transitions, and future studies will examine the effect of such features on fold–thrust structures.

The models suggest a mechanism by which thrust faults can step stratigraphically up from a zone of distributed, bedding-parallel shear décollement. Thrust ramps (step-ups) are nucleated as folds in an incompetent stratigraphic unit beneath anticlinal buckles of the overlying competent unit. The inverted limbs tear to faults

which propagate through the competent unit and the folds are subsequently transported and modified by fault-bend or fault-propagation mechanisms. This relationship, like those just listed, is dependent on properties of the stratigraphic succession. It is favoured where a prominent competent plate lies between relatively thick incompetent units. It provides a possible explanation for the apparent spatial periodicity ('wavelength') of thrust ramps in many fold–thrust belts.

EXPERIMENTAL SET-UP

The centrifuge apparatus, model geometry and scaling

The Experimental Tectonics Laboratory at Queen's University is equipped with a centrifuge that is capable of subjecting two specimens, each measuring 127 × 76 mm in plan and up to 51 mm in depth, to accelerations as high as 20,000 **g** (described by Dixon & Summers 1985).

Dimensions and initial configuration of models are shown in Fig. 1. The 'foreland' portion is made up of three stratigraphic units (I–III), each a finely laminated multilayer constructed of Plasticine (Harbutt Gold Medal Brand) and silicone putty (Dow-Corning Dilatant Compound 3179). These materials are reasonable mechanical analogs for interbedded limestone–shale or sandstone–shale undergoing ductile deformation at shallow crustal levels (Dixon & Summers 1985). This is shown in Fig. 2, in which the rheological properties of the model materials and of such prototype geological materials are compared, given the chosen model ratios (Table 1).

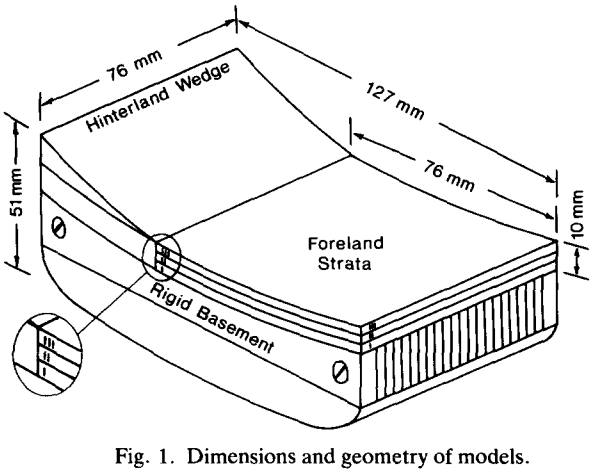

Fig. 1. Dimensions and geometry of models.

Silicone putty deforms in a ductile manner over the full range of conditions encountered in the test and model experiments. Plasticine is ductile at low strain rates, but at higher rates (and possibly at higher values of total strain) it exhibits failure on discrete shear surfaces. In centrifuge tests of failure of model embankments, Stevens (1983) determined that Gold Medal black and white Plasticine failing on discrete shear surfaces has a cohesive shear strength of about 70 kPa at strain rates of approximately 10−1 s−1 (Fig. 2). Evans (1987) conducted triaxial testing of Plasticine at lower strain rates (ductile behaviour). She found that its shear strength increases by a small amount [about 25% (from approximately 20 to 25 kPa) for Harbutts Gold Medal black and 50% (from approximately 12 to 17 kPa) for Harbutts Gold Medal blue] as the confining pressure increases from 0 to 400 kPa (tests at constant strain rates in the range $1.6 \times 10^{-5}\,s^{-1}$ and $2.5 \times 10^{-4}\,s^{-1}$, and stress measured at 10% strain). Evans measured cohesions of 19 and 12 kPa for black and blue Plasticine, respectively (see Fig. 2). The Gold Medal Plasticine has an appropriate yield strength to simulate plastic deformation of the more competent rock types (limestone, sandstone), but, as will be seen below, in the models presented here it undergoes rather too much ductile strain before localized shear failure on discrete faults is initiated. Its behaviour is also essentially purely cohesive rather than frictional (Coulomb). Nevertheless, the model results provide insight into relationships between folds and thrust faults.

Stratigraphic units can be prepared (Dixon & Summers 1985) with any ratio of thickness of competent (Plasticine) and incompetent (silicone putty) layers. This ratio simulates the limestone/shale or sandstone/shale ratio in prototype rock units, and controls overall bulk competence. Thin laminae give the multilayer a high degree of anisotropy that simulates the bedded character of prototype units. The models represent a substantial improvement in geometric scaling (bedding-plane density) over past model studies: laminae 42–166 μm thick represent prototype beds 8–32 m thick.

This study involves two series of models, with internal stratigraphy as shown in Fig. 3 (Series A, Models F2, F4 and F6, and Series B, Models F7-F10, F13 and F14). In

Table 1. Model ratios

Quantity	Model ratio	Scaled equivalent
Length	$l_r = 5 \times 10^{-6}$	10 mm (model) = 2.0 km (prototype) (height of stratigraphic column)
Specific gravity	$\rho_r = 0.6$	1.45 (model) = 2.40 (prototype) (average for full stratigraphic column)
Acceleration	$a_r = 2.5 \times 10^3$	2500 **g** (model) = 1 **g** (prototype)
Time	$t_r = 10^{-10}$	1 h (model) = 1.15 Ma (prototype)
Stress	$\sigma_r = \rho_r \cdot l_r \cdot a_r = 7.5 \times 10^{-3}$ (calculated from other ratios)	

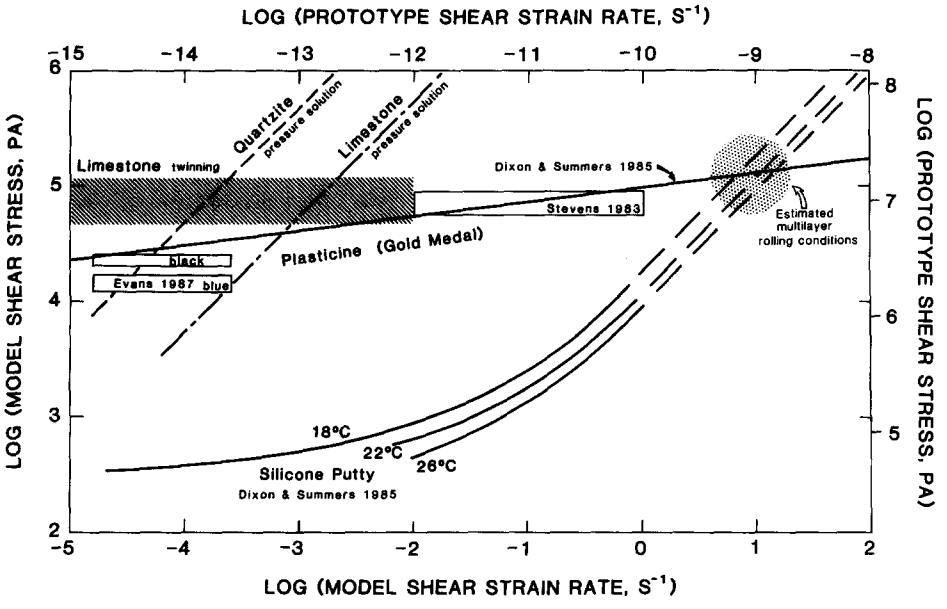

Fig. 2. Stress vs strain rate plot illustrating the rheological behavior of model materials silicone putty and Plasticine deforming by creep (left and bottom axes), and prototype materials limestone (pressure solution or calcite twinning) and quartzite (pressure solution) (right and top axes). The two sets of axes are related by the chosen model ratios (Table 1). Models in this study contain Dow-Corning silicone putty and Harbutt Gold Medal Plasticine. Rheologic data for silicone putty are taken from Dixon & Summers (1985). The solid line is an estimate of behavior of Plasticine (Dixon & Summers 1985) constrained by model slope failure experiments using black and white Gold Medal Plasticine (box labelled Stevens 1983). Triaxial testing of Gold Medal Plasticine by Evans (1987) gave results indicated by the boxes labelled "black" and "blue". See text for discussion. Multilayers are rolled at high strain-rate conditions under which the two materials have equal strength. Model deformation is estimated to involve log strain rates in the range -2 to -4 s^{-1}. The figure is modified from Dixon & Summers (1985).

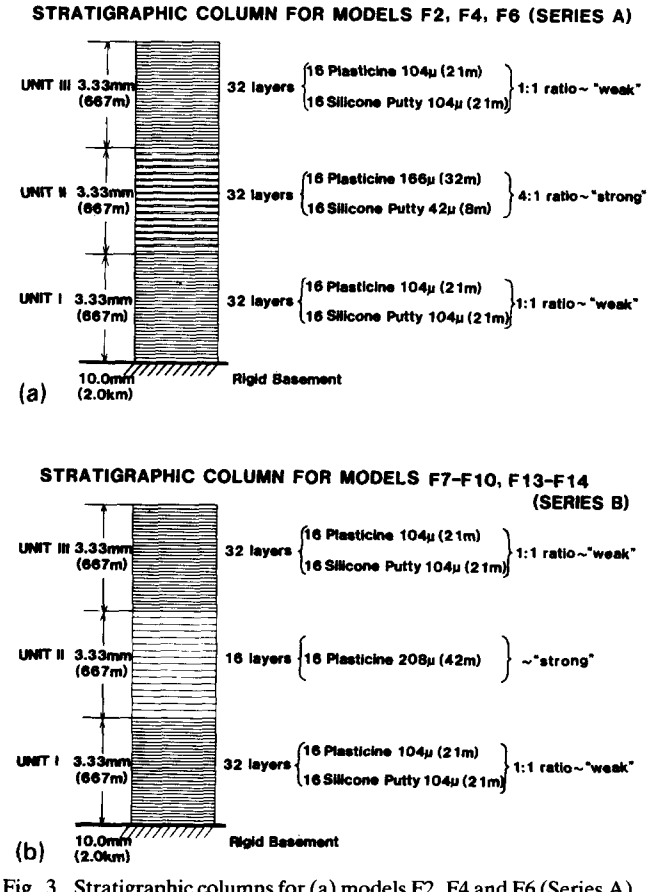

Fig. 3. Stratigraphic columns for (a) models F2, F4 and F6 (Series A), and (b) models F7–F10 and F13–F14 (Series B), with thicknesses of model and equivalent prototype layers.

both series Units I and III consist of 1:1 Plasticine/silicone putty multilayers. Unit II consists of a 4:1 Plasticine/silicone putty multilayer in Series A, whereas it consists entirely of Plasticine of two different colours, without incompetent interbeds, in Series B. Thus the middle unit has lower anisotropy, and higher layer-parallel shear strength and bending resistance, in Series B than in Series A.

The models represent prototype sequences characterized by a tripartite stratigraphic succession of basal and upper, well-laminated and incompetent units, and a middle, somewhat more isotropic and competent unit. They simulate the full stratigraphic succession of some foreland belts (see below); they may be taken as representing portions of the section in other belts.

The models overlie a rigid base composed of aluminium plates, each 0.125 inch (3.18 mm) thick, which can be separated for serial sectioning (Fig. 1). The top surface of the base is a circular cylinder, with a radius of 13.0 inches (330 mm) concentric about the rotation axis of the centrifuge. It constitutes a horizontal basement for the models, an equipotential surface relative to the centrifugal force field.

The basal lamina of the foreland package in all models is composed of Plasticine, lying directly on the aluminium base. Thus the model foreland does not have a weak basal layer that would be analogous to evaporites that underlie, for example, the Jura (Laubscher 1977) or Zagros (Coleman-Sadd 1978) fold belts. The basal décollement horizon in contact with the basement is as

strong as the bulk of the foreland package, although Unit I as a whole is weaker than the full stratigraphic pile.

Mechanism of compression of the models

Layer-parallel compression is applied to the foreland by gravitational spreading of a 'hinterland' wedge (see Fig. 1) of Plasticine. With the geometry shown in Fig. 1, spreading starts when the centripetal acceleration reaches about 2500 **g**. The wedge loses gravitational potential as it spreads; the acceleration must be increased to keep the deformation going during each stage of an experiment. A dynamic analysis of the compression supplied by the wedge is given below.

All experiments were run at 22–24°C. The models are deformed in stages so that the evolution of the structures can be studied. The term "stage" as used here refers to an episode of deformation in the centrifuge rather than to a distinctive portion of the structural evolution of a model. After each stage the hinterland is rejuvenated by addition of a thin wedge of Plasticine (50 mm long, tapered from 5.0 to 0.5 mm). Series-A models were deformed in three stages (Table 2), F2 through stage I, F4 through stages I and II, and F6 through all three stages. Models F7–F10 (Series B) were subjected to a similar sequence of four stages (I–IV; Table 2).

Models F13 and F14 (Series B) both had six stages (I–VI, Table 2), and were sectioned longitudinally between stages. The longitudinal cuts, being parallel to the transport and shortening direction, have no significant effect on the evolution of these models, although reassembly cannot be precise enough to allow successive cuts along the same plane. Sections cut after a particular stage were spaced sufficiently far apart (0.375 inch or 9.5 mm) so that two more cuts could be made after later stages in the intervening blocks. The structures are sufficiently cylindrical that even the smallest folds can be traced between adjacent sections. Thus the kinematic evolution can be followed in detail.

The wedge spreads by failing on a rotational slip surface (a listric normal fault) that roots at its bottom, front edge, and that crops out at its top, rear edge. The leading face of the wedge remains almost vertical during failure, although it tends to ride over the basal portion of the multilayer at advanced stages of deformation (see below, Figs. 7, 8 and 9). The vertical wedge front is a somewhat unnatural boundary condition. It gives rise to localized deformation of the model foreland for which there may be no realistic natural prototype. Nevertheless, the bulk of the foreland, beyond about 10 mm from the wedge front, is not affected by the boundary. The spreading wedge is employed as a tectonic 'black box' that compresses the layered section from one end, simulating compression that could arise from 'gravity glide', from 'gravitational spreading' in the hinterland (Price 1973) or within the fold–thrust belt (Elliott 1976) or from "push from the rear" (Chapple 1978, Davis *et al.* 1983). The layered portion of the models represents a sedimentary pile through which the deformation front, or toe, of a fold–thrust belt migrates.

Dynamics of the compression

It is difficult to estimate precisely the magnitude of the average horizontal stress that is applied to the model 'foreland' by the spreading wedge, both because this stress varies in time due to progressive collapse of the wedge and because the shear strength of the Plasticine is not precisely known (see above and Fig. 2; also Dixon & Summers 1985). A rough estimate can be obtained by applying the conventional analysis of a simple rotational slump (e.g. Terzaghi and Peck 1967) against a buttress (see Fig. 4). In this analysis the slip surface in the wedge is assumed to have a perfect circular shape (which in fact it does not), and the failed slump block is assumed to be rigid (in fact the non-circular shape of the failure surface requires internal deformation of the slump block). In view of the uncertainties involved, a more sophisticated analysis is not deemed to be worthwhile.

Table 2. Run records

Stage	Run-up (s)	Time at 4000 **g** (s)	Run-down (s)
Series A (Models F2, F4, F6)			
I	300	300	410
II	300	150	410
III	300	300	410
Series B (Models F7–F10)			
I	275	200	410
II	275	150	410
III	275	300	410
IV	275	600	410
Series B (Models F13–F14)			
I	275	200	400
II	275	150	400
III	275	300	400
IV	275	600	400
V	275	600	400
VI	275	900	400

*Including ~100 s from 2500 **g** to 4000 **g**.

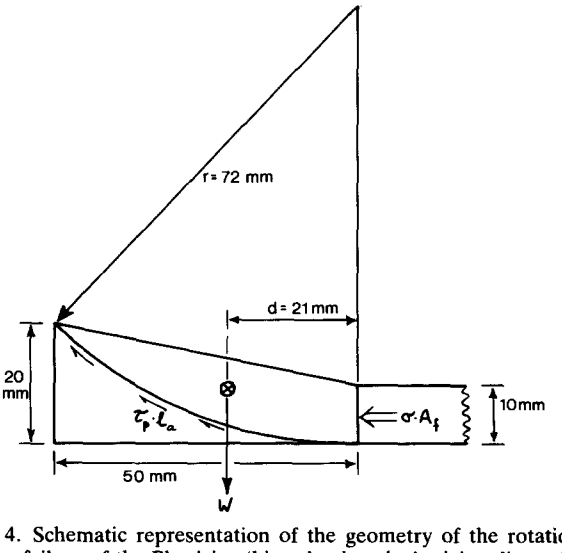

Fig. 4. Schematic representation of the geometry of the rotational slump failure of the Plasticine 'hinterland wedge', giving dimensions used in the dynamic analysis (see text and Fig. 5).

At equilibrium, just before failure, the force that tends to make the slump block slide must be balanced by a resisting shear force along the base of the slump block plus a horizontal compressive force against the buttress (the end of the "foreland" stratigraphic pile). In the following analysis the forces are calculated for 1 m of strike length

$$W \cdot d = \rho_P \cdot A_w \cdot \mathbf{g} \cdot a \cdot \mathrm{d}$$

(driving force)

$$= (\tau_P \cdot l_a \cdot r) + (\sigma_f \cdot A_f),$$

(resisting basal shear force on slump block) + (resisting horizontal compression on foreland)

where W (weight of slump block) $= \rho_P \cdot \mathbf{g} \cdot a$

ρ_P (density of Plasticine) $= 1.7 \times 10^3\ \mathrm{kg\ m^{-3}}$

A_w (cross-sectional area of slump block) $= 4.41 \times 10^{-4}\ \mathrm{m^2}$

$\mathbf{g}$ (gravitational acceleration) $= 9.8\ \mathrm{m\ s^{-2}}$

a = centrifuge acceleration factor

d (lever arm of slump block) $= 2.1 \times 10^{-2}$ m (see Fig. 4)

τ_P (shear strength of Plasticine) $= 4 \times 10^4$ Pa (approx.). This value is intermediate between values determined by Stevens (1983) and Evans (1987); see above

l_a (length of arc of slump block) $= 5.5 \times 10^{-2}$ m (see Fig. 4)

r (radius of slump failure surface) $= 7.2 \times 10^{-2}$ m (see Fig. 4)

σ_f = average stress against foreland buttress

A_f (area of end of foreland buttress) $= 10^{-2}\ \mathrm{m^2}$.

The force that tends to move the slump block is proportional to the centrifuge acceleration. The resisting shear force along the base of the slump is dependant on the geometry of the slump block and the shear strength of the Plasticine. The shear strength is in turn dependant on the strain rate and the centrifuge acceleration in that this affects the confining pressure on the slip surface. However, as the pressure and strain-rate effects are small (see above) they will be neglected and the shear strength will be assumed to have a value of 40 kPa (a value intermediate between values determined by Stevens 1983 and Evans 1987; see above). By observing the value of acceleration in the centrifuge required to initiate failure of the wedge, we can estimate the magnitude of the compression applied by the foreland buttress at that instant.

The variations of the three force components as functions of centrifuge acceleration are shown in Fig. 5. The driving-force and basal-shear resistance components are equal at approximately 1000 **g**; at higher accelerations, the slump block would slide were it not restrained by the foreland buttress. Failure is observed to commence once the centrifuge acceleration reaches approximately 2500 **g**; thus the maximum resisting force provided by the foreland buttress is approximately 227 N. This corresponds to a horizontal compressive stress (in excess of lithostatic), averaged over the full model stratigraphic column, of 2.3×10^4 Pa.

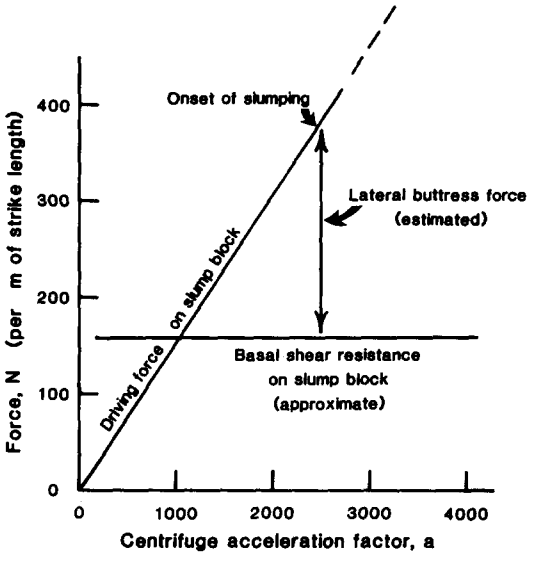

Fig. 5. Plot of forces acting on the 'hinterland' slump block as a function of centrifuge acceleration factor (per metre of strike length of the wedge). Driving force is calculated from weight of slump block and rotational moment. Basal shear resistance is approximated on the basis of estimated shear strength of Plasticine and assuming purely cohesive behaviour. Lateral buttress force applied by the 'foreland' portion of the model is the difference between the other two curves. Slumping of the wedge commences at approximately 2500 **g**. See text for details.

This stress is just sufficient to initiate shortening of the foreland buttress. For comparison with the data in Fig. 2 it is necessary to convert this compressive differential stress to an equivalent shear strength value ($\sim 1.1 \times 10^4$ Pa assuming purely cohesive behaviour). Note that this value falls between the Plasticine and silicone putty curves on Fig. 2. It thus corresponds to a reasonable average strength of the composite, multilayered foreland section.

The precision of the dynamic scaling achieved in the models can be analysed in terms of the so-called Smoluchowski Number (Ramberg 1981), the ratio of gravity stress (S_g) to tectonic stress (S_t). In the model, at a point just in front of the hinterland wedge and at mid-height ($h = 5$ mm) in the foreland pile, the Smoluchowski Number at onset of deformation is

$$\mathrm{Smol}_{\mathrm{model}} = \frac{S_g}{S_t} = \frac{\rho \cdot h \cdot \mathbf{g} \cdot a}{\Delta\sigma}$$

$$= \frac{1.45 \times 10^3 \cdot 5.0 \times 10^{-3} \cdot 9.8 \cdot 2500\ (\mathrm{Pa})}{2.3 \times 10^4\ (\mathrm{Pa})}$$

$$= 7.7.$$

For correct dynamic scaling, the model and natural prototype must have the same value of this ratio. In order for the Smoluchowski Number to have this value

at the equivalent point in the prototype, the tectonic stress at that depth (h = 1.0 km) would be

$$S_t = \frac{S_g}{\mathrm{Smol}_{proto}} = \frac{\rho \cdot h \cdot \mathbf{g}}{7.7}$$

$$= \frac{2.4 \times 10^3 \cdot 10^3 \cdot 9.8\,(\mathrm{Pa})}{7.7}$$

$$= 3.0\,\mathrm{MPa}\,(30\,\mathrm{bar}).$$

This value is below, but probably within one order of magnitude of, realistic levels of differential stress required to drive deformation of thrust belts. For example, Ranalli (1987) estimates that an accretionary wedge with a strong base must have a yield strength $\leq$10 MPa in order to maintain a reasonable surface slope.

It is important to emphasize that the foregoing analysis is presented as a rough approximation of the dynamics of the model experiments described. Furthermore, the calculation applies only at the commencement of failure of the 'hinterland wedge'. Once failure is under way, the wedge geometry changes, the acceleration is gradually increased to 4000 **g**, and the strength of the foreland buttress changes in a complex way as the microlaminations yield by layer-parallel shortening, inter-layer slip, folding and faulting (see below).

EXPERIMENTAL RESULTS

Surface deformation patterns

Figure 6 illustrates the propagation of folds across the surface of models of Series A during the three stages. Deformation during a given stage is quite reproducible (compare Figs. 6a, b & d, which show stage I; and Figs. 6c & e, which show stage II). Series-B models exhibit similar propagation patterns.

Folding of the surface layers nucleates ahead of the wedge and propagates towards the 'craton' end of the models. Propagation occurs by nucleation of new periclinal folds ahead of older, higher-amplitude folds. Individual small-scale folds grow in amplitude and hinge-line length simultaneously, until they encounter other propagating folds. The result is an en échelon array of periclines. This pattern of elongate, doubly-plunging or periclinal folds is common in fold–thrust belts (e.g. U.S. Appalachians, Gwinn 1964; Jura, Pierce 1966; Canadian Rocky Mountains, Thompson 1979).

The anticline adjacent to the wedge front is much larger than other surface folds. It overlies an intensely-deformed packet of folds in Unit I and a large anticline in Unit II (see Fig. 7) that result from the wedge-front boundary condition. The surface layers of Unit III undergo outer-arc stretching over this anticline; conjugate normal faults that accommodate the stretching can be seen to crop out in Figs. 6(e) & (f). By the end of stage III the entire surface of the model is saturated with folds, and the rigid boundary at its 'craton' end influences the deformation.

Fold hinges (and the wedge front) are arcuate in plan (convex towards the direction of movement) due to drag against the side walls of the model chamber. The wedge spreads like a valley glacier; the listric normal fault on which it fails is spoon-shaped, concave in the direction of movement. The arcuate fold pattern is a manifestation of differential shortening of the layered portion of the models. The folds near the lateral boundaries exhibit oblique orientations relative to the transport direction from the earliest stages (as can be seen from examination of the edges of the models at stage I in Figs. 6a, b & d). They did not simply form perpendicular to the transport direction and then undergo passive rotation; rather, they formed at oblique angles as a result of combined longitudinal shortening and shear parallel to the edges of the models. The folds near the margins of the models exhibit a deformation pattern like that described by Fischer & Coward (1982), and ascribed by them to differential movement or 'surge' of the thrust sheet (see Fig. 12). Folds can also develop in arcuate patterns due to differential basal drag, for example because of the local presence of a salt horizon (Davis & Engelder 1985), but this mechanism does not apply in the present case as the models have laterally uniform basal layers.

Internal deformation in Series A

The models were sectioned parallel to their long dimension (transverse to the fold and fault structures). Sections through models of Series A (Fig. 7) show that the style of deformation varies with depth. Unit III exhibits upright folds with a wavelength of approximately 3 mm. After stage I, these folds have rounded, concentric form; they die out downwards onto the top surface of Unit II. In stages II and III they amplify and become more angular. They also influence the upper layers of Unit II more strongly.

At the earliest stage of deformation, Unit II undergoes homogeneous, layer-parallel shortening and vertical thickening but shows little sign of buckling. By stage II, a long-wavelength (approximately 15 mm) buckling of Unit II is evident (Fig. 7, F4-II).

In contrast to Unit III, Unit I exhibits shorter-wavelength folds that are first inclined and later overturned towards the 'craton'. They die out downwards; there is more buckle-shortening in the upper part of Unit I than at its base. The differential shortening indicates that Unit I is acting as a zone of distributed décollement above the rigid basement. It is striking that the folds in Unit I occur in isolated packets, separated by undeformed portions of this unit. The packet spacing or wavelength is approximately 15 mm (Fig. 7, F2-I and F4-II). At stage I, the folds in Unit I have very low amplitudes. By stage II it is apparent that the fold packets of Unit I are associated with the long-wavelength anticlines in Unit II.

There are no inherent properties of Unit I that should cause it to deform into localized fold packets; this mode of failure must be a reflection of the boundary conditions

imposed on it by the overlying Unit II, which is a competent layer embedded in a less competent matrix and therefore deforms by buckling with a characteristic wavelength (Biot 1961, Ramberg 1963, 1970). Buckling of competent layers in Unit I begins at a very early stage: folds can be seen after stage I (Fig. 7). They are due to layer-parallel compression applied to the multilayer from one end by the spreading wedge. There must be a monotonic gradient in this layer-parallel stress, decreasing from hinterland to foreland (see, for example, Mandl & Shippam 1981). The monotonic gradient notwithstanding, the layer-parallel stress is large enough to cause buckling in regions c and e (Fig. 7, F2-I), although it is not large enough in regions b and d. The solution to this paradox is that the vertical stress must vary along Unit I, being slightly reduced beneath Unit-II anticlines, relative to beneath synclines (Johnson & Honea 1975). This local reduction produces a differential stress that is relatively larger beneath the Unit-II anticlines than beneath the synclines, and that is sufficient to buckle the layers of Unit I only beneath the anticlines. Thus, buckling of Unit II triggers localized deformation in Unit I. Willis (1984, plate XCIII) also observed "thrust-[ing] developed where pressure is relieved by overarching competent strata". The Unit-II folds are "detachment folds" (Jamison 1987) (see Fig. 13), the Unit-I fold packets accommodating local thickening beneath the anticlines.

As shortening continues, distributed shear within Unit I due to drag along the no-slip basement contact causes Unit-I folds to become more overturned and their axial surfaces more listric. The overturned limbs are stretched. In these models the model materials do not yield by shear failure on discrete surfaces, so true thrust faults are not developed (but see below). However, these structures resemble Heim's (1878) "stretch thrusts". They rise out of décollement horizons, individual silicone putty laminae, above the basement contact, and pass upwards into Unit II where the shortening that they accommodate is dissipated in folds and layer-parallel shortening. In natural prototypes, this structural succession might be followed by thrust–fault imbrication of Unit II as described, for example, by Fischer & Coward (1982).

Internal deformation in Series B

The internal strain patterns and progressive deformation of models of Series B (Figs. 8 and 9) are grossly similar to those of Series A. However, Unit II in Series B lacks incompetent interbeds, and is much more resistant to short-wavelength folding. It undergoes layer-parallel shortening and well-defined long-wavelength buckling that localizes fold packets in Unit I, as in Series A, but it is less affected by the short-wavelength folds of Units I and III. Unit II has a longer wavelength in Series B than in Series A: models F7–F10, F13 and F14 have only three anticlines, whereas models F2, F4 and F6 have four to five. We have not attempted to test theoretical models of buckling by comparing the fold wavelengths observed in the centrifuged models to those predicted by theory (e.g. Biot 1961, Ramberg 1963, 1970, and others).

The packets of folds with listric axial surfaces in Unit I resemble arrays of incipient imbricate thrust faults, especially by stage IV (Figs. 10 and 11). The fold arrays rise out of a décollement horizon just above the basement. In model F10-IV (Fig. 8), some of the shortening that is accommodated by the middle fold packet of Unit I is transferred across Unit II along a narrow kink band that dips towards the hinterland at about 40°. A similar structure in model F14-IV (Fig. 9) subsequently develops into a thrust fault (Fig. 9, F14-V and F14-VI) that ramps upwards through the middle competent unit and then changes its trajectory towards parallelism with the bedding at the base of the overlying, incompetent Unit III. This is best seen in Fig. 9, F14-V, above the left-dipping flank and crest of the Unit-II anticline in the footwall of the fault: the small-scale folds within the lower part of the Unit III are disharmonically offset and verge towards the foreland, indicating foreland-verging décollement in the lowest layers of Unit III. Thus, the fault resembles a typical thrust fault that has flat–ramp–flat geometry (but see below). By stage VI (Fig. 9) the leading limb of the third (rightmost) anticline is also displaced by a thrust fault. Continued motion on these faults could modify the hanging-wall geometry by fault-bend folding. The essence of this model is that ramp positions are predetermined by the folds in the competent member. Because a simple step-up cannot in general solve the room problem beneath a fold of arbitrary shape (Suppe 1985) the step must rise out of a zone of inhomogeneous strain beneath the anticline.

Model F13 evolved in a similar fashion, although its thrust faults developed more symmetrically (see Fig. 10), some verging towards the 'craton' (right) as in model F14, and others verging towards the 'hinterland' (left). The hinterland-dipping faults have shallower dips (22–25°) than the craton-dipping one (35°). This pattern of concurrent forward and back thrusting is characteristic of fold–thrust belts which develop wedge-shaped profiles of low taper (Chapple 1978) as a consequence of a basal unit that is relatively weaker than the bulk of the accretionary wedge. The basal Unit I in Series B is significantly weaker than the average strength of the whole stratigraphic succession. Another contributing factor is the finite length of the model: by stage VI (Figs. 9 and 10) the deformation has propagated throughout the model and the rigid end of the model chamber is felt. At this point the stratigraphic pile is being shortened symmetrically rather than overthrust to the right, and thus forward and back thrusts are both favoured. Models F13 and F14 had identical initial geometries and run histories. Their different final geometries are due to uncontrolled fold and fault nucleation. The Plasticine, although it has the appopriate yield strength to represent the prototype limestone, is capable of undergoing a large amount of ductile strain under these model stress–strain-rate conditions before it fails on discrete shear planes. Therefore, the Unit-II buckle folds in Series B grow to high amplitude before their leading limbs be-

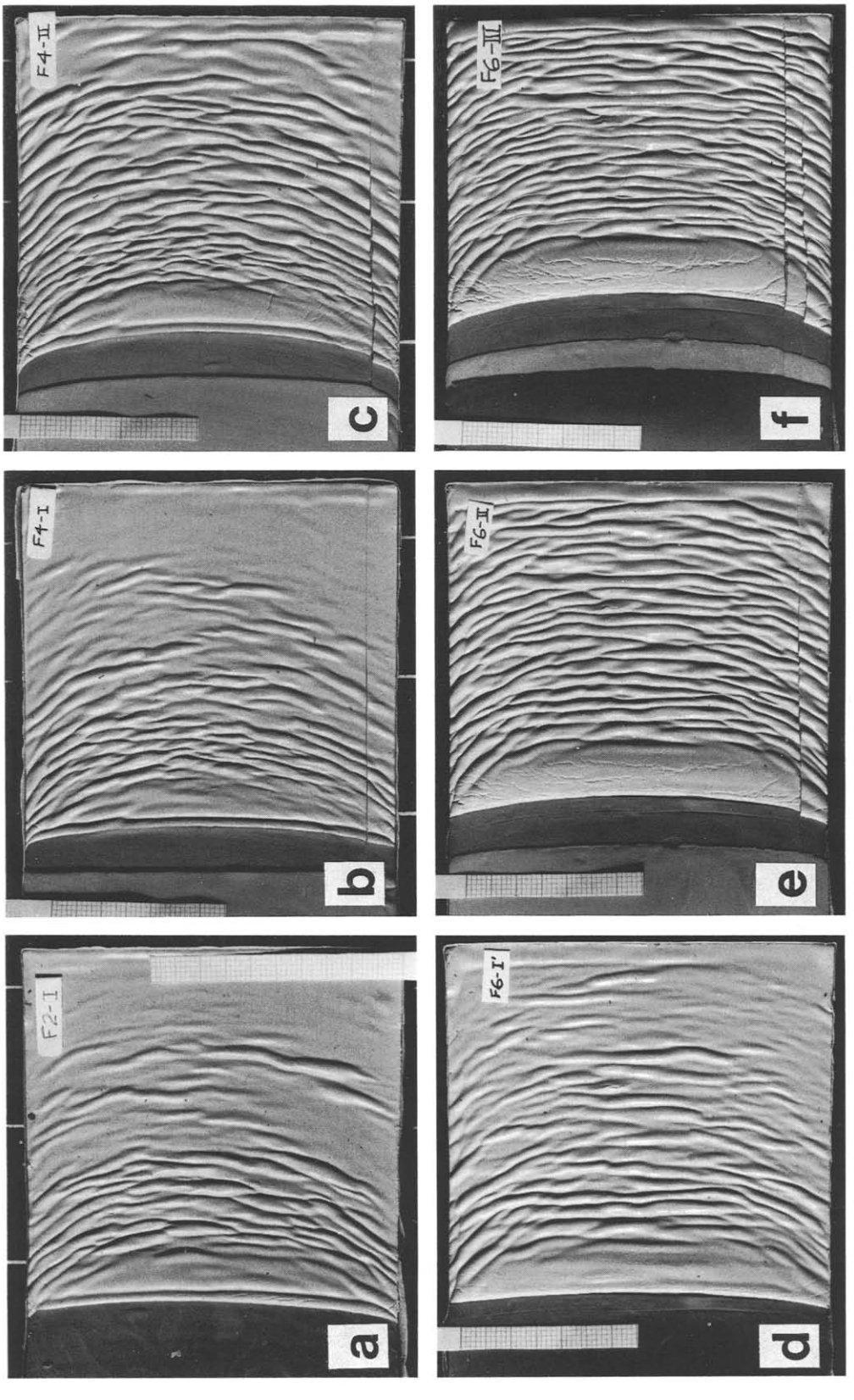

Fig. 6. Surface deformation of models F2, F4 and F6 (Series A) through three stages (I–III) of deformation (oblique lighting from the left). The spreading wedge has advanced from the left. Scale grids in mm.

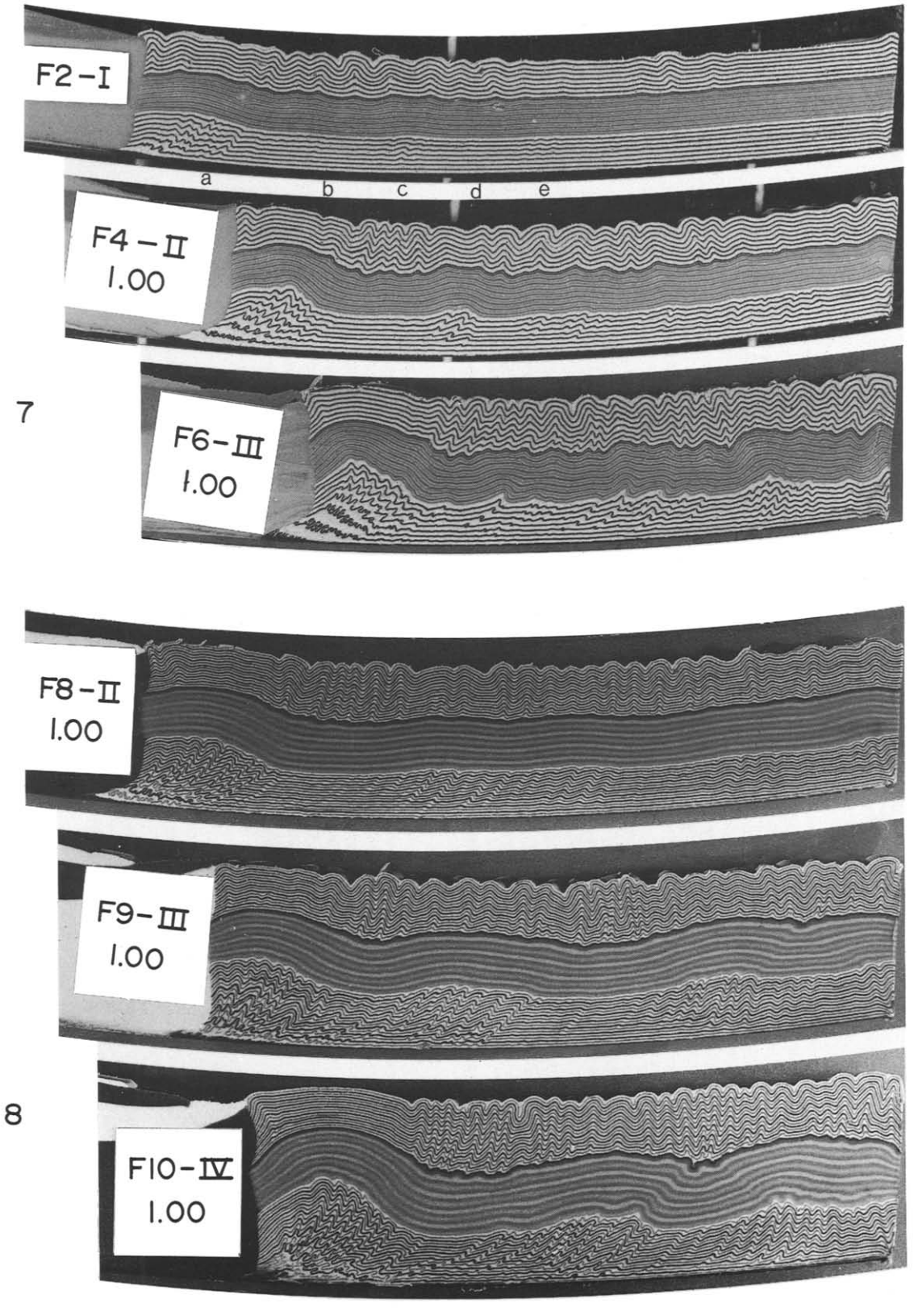

Fig. 7. Profile sections through Models F2-I, F4-II and F6-III, cut at a distance 1.00 inch (25.4 mm) from the near edge of the models. Compression from the left. Label F6-III measures 10 mm wide.

Fig. 8. Profile sections through Models F8-II, F9-III and F10-IV, cut at a distance of 1.00 inch (25.4 mm) from the near edge of the models. Compression from the left. Label F10-IV measures 10 mm wide.

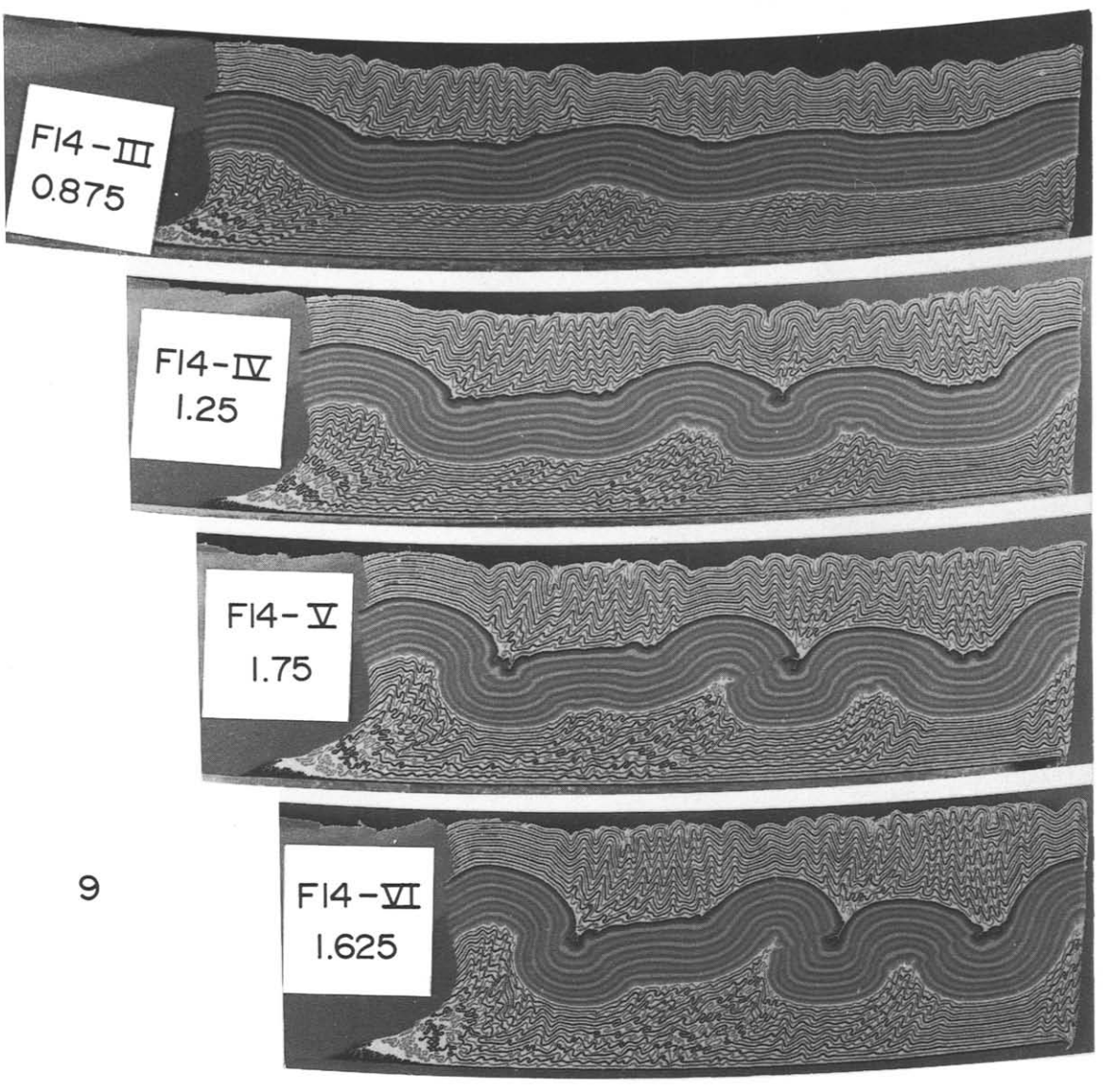

9

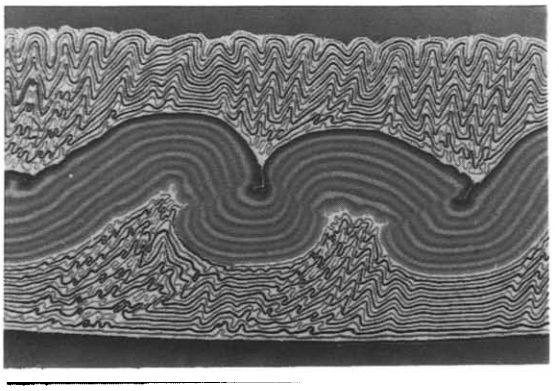

10

Fig. 9. Profile sections through Model F14 after stages III–VI, cut at distances indicated (inches) from the near edge of the models. Compression from the left. Labels measure 10 mm wide.

Fig. 10. Close-up of section 1.625, model F13-VI, showing forward and back thrusts. Compression was from the left.

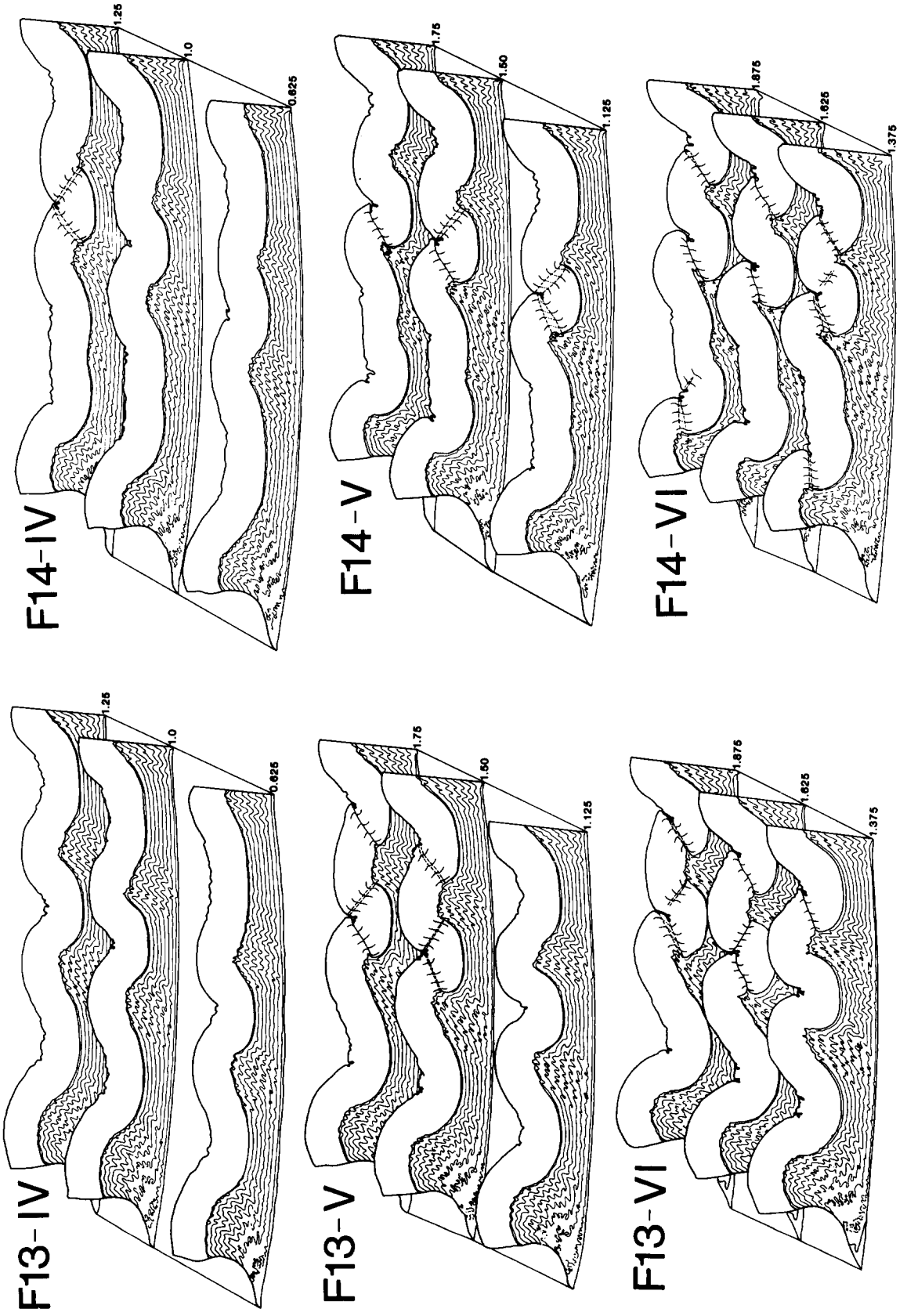

Fig. 11. Line drawings of serial sections through models F13 and F14 at stages IV–VI. In each figure the sections are aligned in correct relative position so as to give an isometric perspective view. Units I and II only are shown; Unit III is omitted for clarity. Figures at the right-hand end of each section indicate the position (in inches) of the section relative to the near edge of the model. The full width of the models is 3.00 inches.

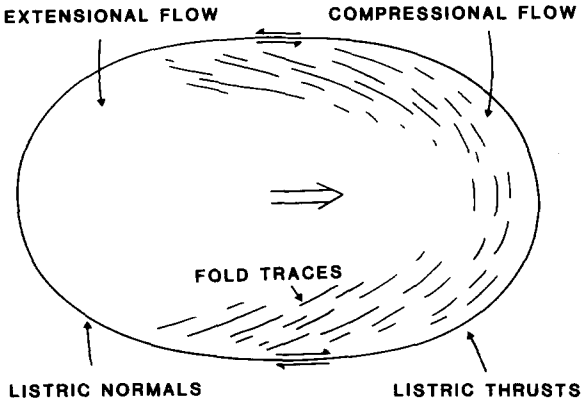

Fig. 12. Sketch map showing the pattern of arcuate fold hinges and listric normal and thrust faults that result from differential displacement ('surge') on a basal décollement (after Fischer & Coward 1982). The structural pattern is comparable to that of the experimental models, in which there is drag on the base and against the sides of the model chamber (see Fig. 6).

come faulted. In a prototype system a low-amplitude (perhaps barely perceptible) buckle-fold might develop a sufficient stress concentration or accumulate enough strain to initiate localized shear failure (as in Mandl & Shippam 1981, Eisenstadt & De Paor 1987).

Three modes of propagation of the thrust ramps bear consideration: (1) from the zone of high strain in the core (Unit I) of an anticline to the top of Unit II and into Unit III; (2) from lower and upper interfaces towards the centre of Unit II; and (3) from the centre of Unit II towards the top and bottom contacts. Close examination of Fig. 9 indicates that the strongest foreland-verging shear and dislocation along overturned fold limbs occurs first in the lowest unit beneath anticlines of Unit II (F14-IV, V and VI). It is difficult to determine whether the offset of Unit II begins at its base or at its top, although in F14-V and F14-VI (Fig. 9) and in F13-VI (Fig. 10) this layer is offset more distinctly at its base than at its upper contact. On the whole, the kinematic evidence supports propagation by the first of the three modes listed above. This is in contrast with the mechanism proposed by Eisenstadt & De Paor (1987), that ramps nucleate within a competent unit and propagate both upwards and downwards in the manner of mode 3. However, their model involves brittle failure of planar layers rather than localized ductile shear following folding.

The three-dimensional geometry and kinematic evolution of models F13 and F14 are shown more clearly in Fig. 11, in which line drawings of serial sections are arranged in their correct relative positions in isometric projection. The lateral continuity of both small and large structures (folds and faults) in Units I and II can be better appreciated in this representation (Unit III is omitted for clarity). The large-scale folds of Unit II persist laterally across the width of the models. They are remarkably cylindrical within the portions of the models shown, although they are arcuate in plan on the scale of the full width of the models due to differential shortening and drag against the side walls of the model chamber. Some of the small-scale folds in Unit I can be traced from one serial section to the next, but in general these folds

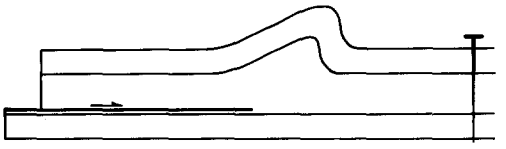

Fig. 13. Profile sketch of a 'detachment' fold (after Jamison 1987). The 'detachment' could be a discrete fault, as shown, or it could be a zone of distributed shear that terminates in the thickened region beneath the anticline.

vary in form over short distances. Nevertheless, fold packets have lateral continuity similar to that of the large folds of Unit II. Thrust faults in Unit II exhibit significant variation in offset along strike, and the lateral propagation of individual faults (Douglas 1958) can be documented by comparing the drawings of successive stages (Fig. 11). Lateral propagation of each fault accompanies progressive tightening of the associated fold and increase in the amount of shear strain in the limb (as discussed in detail by Elliott 1976).

The thrust faults in models F13 and F14 are examples of "smooth-trajectory" thrusts (Cooper & Trayner 1986) which propagate through previously-folded strata, as opposed to 'staircase-trajectory' thrusts which propagate through planar strata with flat–ramp–flat geometry (see Fig. 14). The faults would restore with a staircase geometry onto the undeformed stratigraphic package if conventional techniques of section restoration were applied to the sections illustrated. Nevertheless, we know that the faults formed after a significant amount of folding of the competent Unit II and local ductile deformation of Unit I. The model thrusts would be correctly identified through application of the criteria proposed by Cooper & Trayner (1986) to distinguish smooth-trajectory thrusts from staircase thrusts (footwall geometry and strain state). Fischer & Coward (1982) describe similar fold–thrust relations from the Heilam thrust sheet of northwest Scotland. To restore the model sections correctly, sequential balanced sections which reverse the deformation history would be required (see Cooper & Trayner 1986).

GEOLOGICAL EXAMPLES

The simple, tripartite stratigraphic succession that constitutes the models described above is analogous to the full stratigraphic succession, overlying a mechanically strong, autochthonous crystalline basement, in some natural fold–thrust belts. The kinematic evolution of the models is observed during the experiments: the relative timing of folding and thrusting and the patterns of nucleation and propagation of these structures are known. If the final structural pattern observed in natural fold–thrust belts resembles that of the models, it is worth considering whether the natural belts also underwent the same kinematic evolution as the models. The key question is whether thrusts which ramp through the competent unit were localized by previously-formed folds. This issue may be resolved by observation of

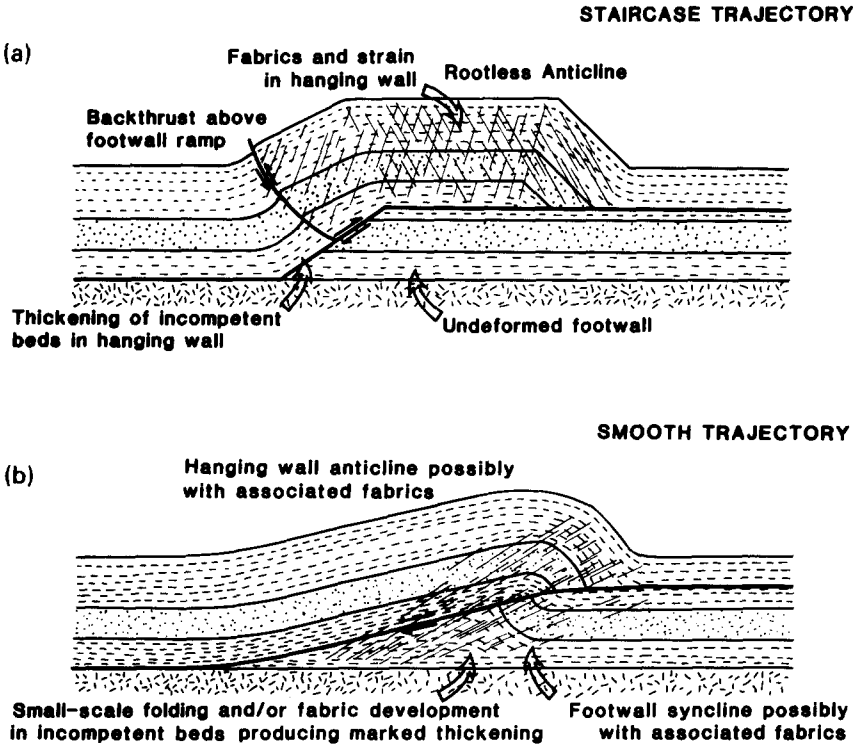

Fig. 14. The principal characteristics of (a) staircase-trajectory and (b) smooth-trajectory thrusts (after Cooper & Trayner 1986).

penetrative strain in the footwalls of ramps and of truncation of mesoscopic folds by thrusts. Two examples of fold–thrust belts which consist of tripartite stratigraphic successions are examined briefly below.

Nappes in the Kilohigok Basin, District of Mackenzie (Canada)

Tirrul (1985, Tirrul & Grotzinger in press) has mapped an Early Proterozoic thin-skinned fold and thrust belt in the Bear Creek Hills area at the south end of Bathurst Inlet (District of Mackenzie, N.W.T., Canada; see Fig. 15). Strata of the Western River Formation have been thrust and folded above Archean basement rocks of the Slave craton. Western River units resemble mechanically the models of Series A. Unit 1 is a well-bedded sequence with moderate competence overall, high anisotropy, and a total thickness of about 400 m. It comprises basal quartz–pebble conglomerate and orthoquartzite (Unit 1a), argillite with carbonate interbeds (1c), interbedded argillate, quartzite and stromatolitic dolomite (1f), and carbonate–mudstone rhythmites (1g). Unit 2a, initially approximately 75 m thick, is incompetent and anisotropic. It is dominantly pelite, with sandy laminations throughout and a few thick interbeds of subarkose near the base. Unit 2e is overall the most uniform and competent in the succession. It comprises 750 m of thickly-bedded subarkose with subordinate interbedded pelite. Unit 3a consists of more than 600 m of incompetent argillite with no sandstone beds. The succession may be approximated by a rigid basement; a lower, incompetent yet well-laminated unit (Units 1 and 2a); a middle, competent unit (Unit 2e); and an upper, incompetent unit (Unit 3a).

Most of the structural geometry of Bear Creek Hills can be ascribed to a phase (D_2) of thin-skinned thrusting and folding. D_2 structures plunging 30–42° to the southwest are projected in Fig. 15(b). At high structural levels, D_2 folds in Unit 2e have aggregate profiles which approach chevron geometry, are upright or steeply inclined towards the northwest, and have interlimb angles which generally exceed 90°. Cleavage is weakly developed. Where axial surfaces are traced to deeper levels, their dips progressively decrease. In the case of some anticline–syncline pairs, axial surfaces meet thrust faults at depth; the faults accommodate shortening strain at depth that is taken up by buckling at higher levels. Cleavage is more strongly developed at depth, and folds, even in the most competent dolomite of Unit 1f, are tighter. The basal detachment, within Unit 1c pelite, separates overlying rocks, which are ubiquitously and tightly folded, from beds beneath, which are only gently folded. The succession beneath the detachment displays D_2 cleavage but is not imbricated. The upper part of the underlying basement also contains traces of the D_2 cleavage. These relationships suggest that the sedimentary cover was bonded to the basement prior to thrusting; there was no prominent weak horizon at the contact that could serve as a strain buffer to allow the basement to remain uninvolved.

D_2 structures of Bear Creek Hills exhibit a vertical transition from large, open and upright folds in the competent Unit 2e to overturned folds in the more highly strained incompetent Unit 2a, and highest-order

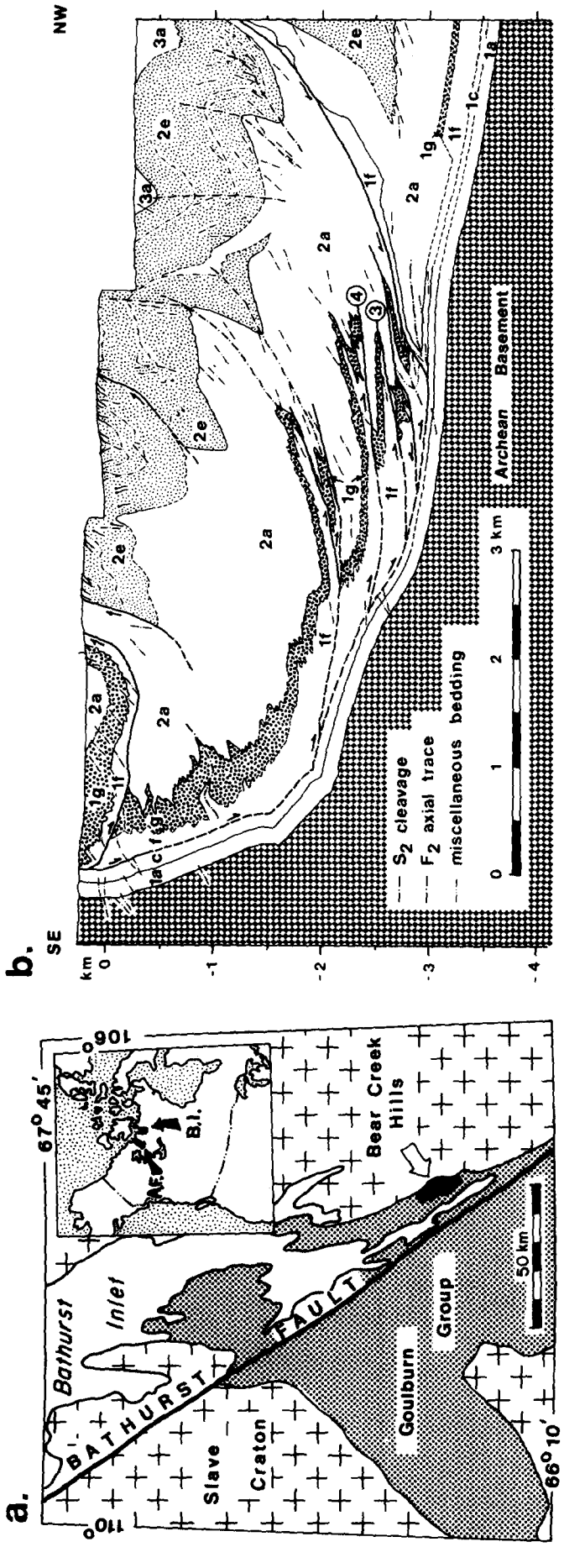

Fig. 15. (a) Location of Bear Creek Hills area, Kilohigok Basin, District of Mackenzie (Canada). Inset shows location of Bathurst Inlet (B.I.) and Asiak Foreland thrust–fold belt (A.F.). (b) Down-plunge projection of Bear Creek Hills fold–thrust structures, with the effects of later (D_3) faulting (see Tirrul 1985) removed. Contacts dashed where surface data unavailable. See text for key to lithological units.

folds and thrusts in Unit 1, strongly resembling the structures that developed in the models of Series A (compare Fig. 15b with Fig. 7). Major upright anticlines in Unit 2e are underlain by major thrusts that imbricate Units 1c–g and the lower part of Unit 2a (Fig. 15b). We suggest that this relationship had the same origin in Bear Creek Hills as in the models: buckling of the competent unit localized thickening and thrust ramping in the underlying incompetent layer. The thrusts must have formed in previously-folded rocks, as they commonly truncate tight NW-verging D_2 folds (e.g. faults 3 and 4 in Fig. 15b). Alternate hypotheses of simple fault-propagation folding or drag-folding can be ruled out.

Asiak Foreland thrust and fold belt, District of Mackenzie, Canada

In Asiak Foreland thrust–fold belt, Wopmay Orogen, most of a 1.9 Ga supracrustal continental margin prism has been detached from its basement, shortened and translated eastwards with respect to the Slave Craton during the Calderian Orogeny (Tirrul 1983, Hoffman & Bowring 1984). The deformed wedge is characterized by a tripartite stratigraphic succession: Odjick Formation, dominantly pelite with thin quartzite interbeds (lower half) and well-bedded mature quartzite (upper half) in aggregate 0.7–1.5 km thick; Rocknest Formation, thickly inter-bedded dolomite and dololutite, 1 km thick; and the Recluse Group consisting of up to 400 m of laminated pelite overlain by more than 1 km of greywacke turbidites. This stratigraphic succession is approximated by the models of Series B, where Unit II is an analog for the Rocknest Formation, bracketed by significantly less competent, but well-layered units above and below.

Asiak Foreland thrust–fold belt displays a variety of thick-skinned structures (Fig. 16), many of which are reproduced in Series B. Like the models, the highest structural level consists of upright chevron folds of greywacke turbidites. Longer wavelength folds and regularly spaced Rocknest–Odjick imbricates characterize intermediate levels. These thrusts rise out of a décollement 100–300 m above the basement, and transport penetratively strained, tightly-asymmetrically folded lower Odjick on hanging-walls. The forward and back thrusts that cut up-section through the competent Unit II in models F14 (Fig. 9) and F13 (Fig. 10) resemble the forward and back thrusts that imbricate the Rocknest (Fig. 16) The displacement on the model faults, like that of the natural ones, is dissipated in bedding-glide on top of the competent unit and in folding of the overlying incompetent strata. These similarities suggest that many of the thrust faults, which imbricate and have caused fault-bend folding of the Rocknest Formation (Tirrul 1983), could have nucleated in zones of high strain and overturned folding in the Odjick Formation at sites beneath incipient long-wavelength anticlines in the Rocknest. This hypothesis is difficult to test; critical evidence that would demonstrate whether folding predated thrust-faulting is obscured by the relative paucity of Odjick Formation outcrops and its lack of easily-recognized internal stratigraphy at the scale of mapping done to date.

The occurrence of both forward and back thrusts in Asiak thrust–fold belt led Tirrul (1983) to interpret it to have formed as a wedge of low taper, as a consequence of its having a relatively weak décollement unit. A similar relationship exists in series B models, of which model F13 developed both forward and back thrusts (Figs. 10 and 11).

CONCLUSIONS

Folding of a competent unit can nucleate folds which develop into thrust ramps in an underlying incompetent unit, by localizing strain (small-scale folding and faulting) beneath the anticlines of the competent unit. This relationship emphasizes the control of stratigraphic succession over structure, and provides an alternate explanation for the spatial periodicity of thrust ramps (contrast with Mandl & Shippam 1981, Bombolakis 1986 and Mulugeta & Koyi 1987).

The thrust faults that form by this mechanism have a trajectory through the folded strata that resembles flat–ramp–flat or staircase geometry, the faults transecting

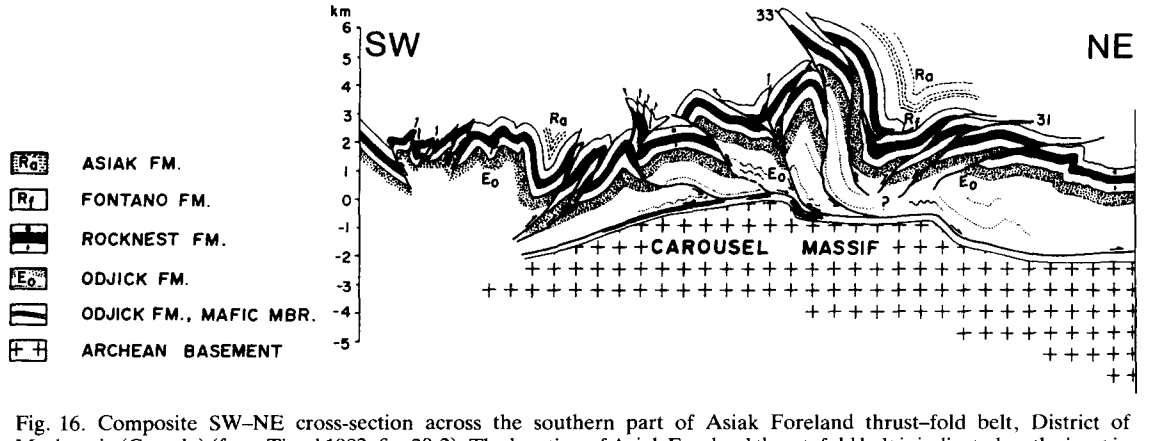

Fig. 16. Composite SW–NE cross-section across the southern part of Asiak Foreland thrust–fold belt, District of Mackenzie (Canada) (from Tirrul 1983, fig. 29.2). The location of Asiak Foreland thrust–fold belt is indicated on the inset in Fig. 15(a).

the competent stratigraphic units at a steep angle and the incompetent units at a shallow angle. However, as the folding occurred before the faulting, the faults in fact propagated along a relatively smooth trajectory. The distribution of strain in both footwalls and hanging-walls of thrust faults provides evidence that detachment folding pre-dated faulting of the middle competent unit. Increasing displacement on the thrusts would modify the hanging-wall structure by gentle fault-bend folding. Thus the structures in the models are the combined result of sequential detachment folding, smooth-trajectory fault propagation and fault-bend folding. This complex evolution is to be expected in natural fold–thrust belts as well; simple, single-mechanism processes are unlikely. The natural examples cited (Bear Creek Hills and Asiak Foreland fold-thrust belts) are characterized by a tripartite stratigraphic succession and exhibit structural relationships that are similar to those seen in the models.

The pronounced foreland vergence of folds in the basal unit of the models is found in many natural fold–thrust belts, including those mentioned above, but it is lacking in others such as the Jura (Buxtorf 1915), the Zagros Gently Folded zone (Colman-Sadd 1978) and the Parry Islands Fold Belt (Fox 1983), which have a prominent weak stratum of salt or shale above the rigid basement. Unpublished models similar to those presented here, but containing a basal layer of silicone putty 0.5–1.0 mm thick, tend to form folds that are upright throughout the section. A thick ductile layer absorbs the shear strain between cover and basement, flows easily into anticlinal cores to alleviate 'room' problems, and inhibits the mechanism of thrust–fault nucleation outlined here.

Acknowledgements–The late Rein Tirrul contributed greatly to this study in its early stages, particularly by providing details of the structural characteristics of the natural examples described here and pointing out the similarities to the models. The models and the dynamic analysis are the responsibility of the first author. Herwart Helmstaedt read the manuscript and made suggestions for its improvement. The paper has benefited greatly from thorough reviews by Chris Talbot, Peter Cobbold and Sue Treagus. Sue Treagus is thanked for asking the pointed question about the modes of propagation of the thrust ramps. Melanie Haggart assisted by drafting some of the figures, notably Fig. 11, and Elizbet Rusak-Mazur made the photographic prints. The Natural Sciences and Engineering Research Council of Canada has funded the construction and operation of the Experimental Tectonics Laboratory at Queen's University.

REFERENCES

Berger, P. & Johnson, A. M. 1980. First-order analysis of deformation of a thrust sheet moving over a ramp. *Tectonophysics* **70**, T9–T24.

Biot, M. A. 1961. Theory of folding of stratified viscoelastic media and its implications in tectonics and orogenesis. *Bull. geol. Soc. Am.* **72**, 1595–1620.

Bombolakis, E. G. 1986. Thrust-fault mechanics and origin of a frontal ramp. *J. Struct. Geol.* **8**, 281–290.

Boyer, S. E. & Elliott, D. 1982. Thrust systems. *Bull Am. Ass. Petrol. Geol.* **66**, 1196–1230.

Bucher, W. H. 1956. Role of gravity in orogenesis. *Bull. geol. Soc. Am.* **67**, 1295–1318.

Buxtorf, A. 1915. *Prognosen und Befunde beim Hauenstein Basis und Grenchenbergtunnel und die Bedeutung der letzeren für die Geologie des Juragebirges. Naturforsch. Gesell.*, Vol. 27. Verhandl, Basel.

Cadell, H. M. 1889. Experimental research in mountain building. *Trans. R. Soc. Edinb.* **31**, 337–357.

Chapple, W. M. 1978. Mechanics of thin-skinned fold-and-thrust belts. *Bull. geol. Soc. Am.* **89**, 1189–1198.

Colman-Sadd, S. P. 1978. Fold development in Zagros Simply Folded Belt, Southwest Iran. *Bull Am. Ass. Petrol. Geol.* **62**, 984–1003.

Cooper, M. A. & Trayner, P. M. 1986. Thrust-surface geometry: implications for thrust-belt evolution and section-balancing techniques. *J. Struct. Geol.* **8**, 305–312.

Dahlstrom, C. D. A. 1969. Balanced cross sections. *Can. J. Earth Sci.* **6**, 743–757.

Dahlstrom, C. D. A. 1970. Structural geology in the eastern margin of the Canadian Rocky Mountains. *Bull. Can. Petrol. Geol.* **18**, 332–406.

Davis, D. & Engelder, T. 1985. The role of salt in fold/thrust belts. *Tectonophysics* **119**, 67–88.

Davis, D., Suppe, J. & Dahlen, F. A. 1983. Mechanics of fold-and-thrust belts and accretionary wedges. *J. geophys. Res.* **88**, 1153–1172.

Dennis, J. G. & Häll, R. 1978. Jura-type platform folds: a centrifuge experiment. *Tectonophysics* **45**, T15–T25.

De Sitter, L. U. 1956. *Structural Geology*. McGraw-Hill, New York.

Dixon, J. M. & Summers, J. M. 1985. Recent developments in centrifuge modelling of tectonic processes: equipment, model construction techniques and rheology of model materials. *J. Struct. Geol.* **7**, 83–102.

Dixon, J. S. 1982. Regional structural synthesis, Wyoming salient of western overthrust belt. *Bull Am. Ass. Petrol. Geol.* **66**, 1560–1580.

Douglas, R. J. W. 1958. Mount Head map area, Alberta. *Mem. geol. Surv. Can.* **291**.

Eisenstadt, G. & De Paor, G. D. 1987. Alternative model of thrust–fault propagation. *Geology* **15**, 630–633.

Elliott, D. 1976. The energy balance and deformation mechanisms of thrust sheets. *Phil. Trans. R. Soc. Lond.* **A283**, 289–312.

Evans, E. A. 1987. Triaxial testing of Plasticine. Unpublished B.Sc. thesis, Queen's University, Kingston, Canada.

Faill, R. T. 1969. Kink band structures in the Valley and Ridge Province, central Pennsylvania. *Bull. geol. Soc. Am.* **80**, 2539–2550.

Fischer, M. W. & Coward, M. P. 1982. Strains and folds within thrust sheets: an analysis of the Heilam sheet, northwest Scotland. In: *Strain Within Thrust Belts* (edited by Williams, G. D.). *Tectonophysics* **88**, 291–312.

Fox, F. G. 1983. Structure sections across Parry Islands Fold Belt and Vesey Hamilton salt wall, Arctic Archipelago, Canada. In: *Seismic Expression of Structural Styles* (edited by Bally, A. W.). *Am. Ass. Petrol. Geol. Studies in Geology Series* 125, **3**, 54–72.

Guterman, V. G. 1980. Model studies of gravitational gliding tectonics. *Tectonophysics* **65**, 111–126.

Gwinn, V. E. 1964. Thin-skinned tectonics in the Plateau and northwestern Valley and Ridge Provinces of the central Appalachians. *Bull. geol. Soc. Am.* **75**, 863–900.

Hall, Sir J. 1815. On the vertical position and convolutions of certain strata, and their relation with granite. *Trans. R. Soc. Edinb.* **7**, 79–108.

Harris, L. D. & Milici, R. C. 1977. Characteristics of thin-skinned style of deformation in the southern Appalachians, and potential hydrocarbon traps. *Prof. Pap. U.S. geol. Surv.* **1018**, 1–40.

Heim, A. 1878. *Untersuchungen über den Mechanismus der Gebirgsbildung*. Schwabe, Basel.

Heim, A. 1921. *Geologie der Schweiz, II. Die Schweizer Alpen*. Tauchnitz, Leipzig.

Hoffman, P. F. & Bowring, S. A. 1984. Short-lived 1.9 Ga continental margin and its destruction, Wopmay Orogen, northwest Canada. *Geology* **12**, 68–72.

Hubbert, M. K. 1937. Theory of scale models as applied to the study of geologic structures. *Bull. geol. Soc. Am.* **48**, 1459–1519.

Jamison, W. R. 1987. Geometric analysis of fold development in overthrust terranes. *J. Struct. Geol.* **9**, 207–219.

Johnson, A. M. & Honea, E. 1975. A theory of concentric, kink and sinusoidal folding and of monoclinal flexuring of compressible elastic multilayers. Part III, Transition from sinusoidal to concentric-like to chevron folds. *Tectonophysics* **27**, 1–38.

Laubscher, H. P. 1977. Fold development in the Jura. *Tectonophysics* **37**, 337–362.

Mandl, G. & Shippam, G. K. 1981. Mechanical model of thrust sheet gliding and imbrication. In *Thrust and Nappe Tectonics* (edited by McClay, K. & Price, N. J.). *Spec. Publs geol. Soc. Lond.* **9**, 79–98.

McClay, K. R. 1976. The rheology of Plasticine. *Tectonophysics* **33**, T7–T15.

Mulugeta, G. 1988a. Squeeze box in a centrifuge. *Tectonophysics* **148**, 323–335.

Mulugeta, G. 1988b. Modelling the geometry of Coulomb thrust wedges. *J. Struct. Geol.* **10**, 847–859.

Mulugeta, G. & Koyi, H. 1987. Three-dimensional geometry and kinematics of experimental piggyback thrusting. *Geology* **15**, 1052–1056.

Pierce, W. G. 1966. Jura tectonics as a decollement. *Bull. geol. Soc. Am.* **77**, 1265–1276.

Price, R. A. 1973. Large scale gravitational flow of supracrustal rocks, southern Canadian Rockies. In: *Gravity and Tectonics* (edited by De Jong, K. & Scholten, R.). Wiley, New York, 491–501.

Price, R. A. & Mountjoy, E. W. 1970. Geologic structure of the Canadian Rocky Mountains between Bow and Athabasca Rivers—a progress report. *Spec. Pap. geol. Ass. Can.* **6**, 7–25.

Ramberg, H. 1963. Fluid dynamics of viscous buckling applicable to folding of layered rocks. *Bull Am. Ass. Petrol. Geol.* **47**, 484–505.

Ramberg, H. 1967. *Gravity, Deformation and the Earth's Crust.* Academic Press, London.

Ramberg, H. 1970. Folding of laterally compressed multilayers in the field of gravity, I. *Phys. Earth & Planet. Interiors* **2**, 203–232.

Ramberg, H. 1981. *Gravity, Deformation and the Earth's Crust* (2nd edn). Academic Press, London.

Ranalli, G. 1987. *Rheology of the Earth.* Allen & Unwin, Boston.

Reks, I. J. & Gray, D. R. 1983. Strain patterns and shortening in a folded thrust sheet: an example from the southern Appalachians. *Tectonophysics* **93**, 99–128.

Rich, J. L. 1934. Mechanics of low-angle overthrust faulting as illustrated by the Cumberland thrust block. *Bull Am. Ass. Petrol. Geol.* **18**, 1584–1596

Rogers, W. B. & Rogers, H. D. 1843. On the physical structure of the Appalachian chain, as exemplifying the laws which have regulated the elevation of great mountain chains generally. *Ass. Am. Geol. natl Reps*, 474–531.

Stevens, T. A. C. 1983. A centrifuge study of slope stability using Plasticine. Unpublished B.Sc. thesis, Queen's University, Kingston, Canada.

Suppe, J. 1980. A retrodeformable cross-section of northern Taiwan. *Proc. geol. Soc. China* **23**, 46–55.

Suppe, J. 1983. Geometry and kinematics of fault-bend folding. *Am. J. Sci.* **283**, 684–721.

Suppe, J. 1985. *Principles of Structural Geology.* Prentice-Hall, Englewood Cliffs, New Jersey.

Terzaghi, K. & Peck, R. B. 1967. *Soil Mechanics in Engineering Practice* (2nd edn). Wiley, New York.

Thompson, R. I. 1979. A structural interpretation across part of the north Rocky Mountains, British Columbia, Canada. *Can. J. Earth Sci.* **16**, 1228–1241.

Tirrul, R. 1983. Structure cross-sections across Asiak Foreland Thrust and Fold Belt, Wopmay Orogen, District of Mackenzie. *Geol. Surv. Pap. Can.* **84–1B**, 253–260.

Tirrul, R. 1985. Nappes in the Kilohigok Basin, and their relation to the Thelon Tectonic Zone, District of Mackenzie. *Geol. Surv. Pap. Can.* **85–1A**, 407–420.

Tirrul, R. & Grotzinger, J. P. In press. Early Proterozoic collisional orogeny along the northern Thelon Tectonic Zone, N.W.T., Canada: evidence from the foreland. *Tectonics.*

Willis, B. 1894. The mechanics of Appalachian structure. *U.S. Geol. Surv. Ann. Rep.* 13, Part II, 211–282.

Wiltschko, D. V. 1981. Thrust sheet deformation at a ramp: summary and extensions of an earlier model. In: *Thrust and Nappe Tectonics* (edited by McClay, K. & Price, N. J.). *Spec. Publs geol. Soc. Lond.* **9**, 55–63.

Wiltschko, D. V. & Chapple, W. M. 1977. Flow of weak rocks in the Appalachian Plateau folds. *Bull Am. Ass. Petrol. Geol.* **61**, 653–670.